Spatial scale of motion segmentation from speed cues

Daniel R. Mestre [a], Guillaume S. Masson [a,*], Leland S. Stone [b]

[a] *Centre de Recherche en Neurosciences Cognitives, Centre National de la Recherche Scientifique, CNRS UPR 9012, 31 Chemin Joseph Aiguier, 13402 Marseille cedex 20, France*
[b] *Human Information Processing Research Branch, Human Factors Research and Technology Division, NASA Ames Research Center, Moffett Field, CA 94035-1000, USA*

Abstract

For the accurate perception of multiple, potentially overlapping, surfaces or objects, the visual system must distinguish different local motion vectors and selectively integrate similar motion vectors over space to segment the retinal image properly. We recently showed that large differences in speed are required to yield a percept of motion transparency. In the present study, to investigate the spatial scale of motion segmentation from speed cues alone, we measured the speed-segmentation threshold (the minimum speed difference required for 75% performance accuracy) for 'corrugated' random-dot patterns, i.e. patterns in which dots with two different speeds were alternately placed in adjacent bars of variable width. In a first experiment, we found that, at large bar widths, a smaller speed difference was required to segment and perceive the corrugated pattern of moving dots, while at small bar-widths, a larger speed difference was required to segment the two speeds and perceive two transparent surfaces of moving dots. Both the perceptual and segmentation performance transitions occurred at a bar width of around 0.4°. In a second experiment, speed-segmentation thresholds were found to increase sharply when dots with different speeds were paired within a local pooling area. The critical pairing distance was about 0.2° in the fovea and increased linearly with stimulus eccentricity. However, across the range of eccentricities tested (up to 15°), the critical pairing distance did not change much and remained close to the receptive field size of neurons within the primate primary visual cortex. In a third experiment, increasing dot density changed the relationship between speed-segmentation thresholds and bar width. Thresholds decreased for large bar widths, but increased for small bar widths. All of these results are well fit by a simple stochastic model, which estimates the probabilities of having identical or different motion vectors within a local pooling area whose size is the same as that of primate V1 neurons. Altogether, these results demonstrate that speed-based segmentation can function well, even at small spatial scales (i.e. high-spatial frequencies of spatial corrugation) and thereby emphasizes the critical role of a local pooling process early in the cortical motion-processing pathway. © 2001 Elsevier Science Ltd. All rights reserved.

Keywords: Motion perception; Speed segmentation; Speed discrimination; Transparency; Spatial scale; Area V1; Area MT

1. Introduction

Motion segmentation is an essential visual process, by which the visual system uses motion to decompose the retinal image into meaningful pieces, each potentially associated with different objects or surfaces in the environment, and then selectively reassembles them to reconstruct objects and surfaces (see Braddick, 1993; Albright & Stoner, 1995; Braddick, 1997, for reviews).

This critical stage in motion processing is constrained by two mechanisms: a segregation process that detects changes in velocity across space and parses the image into regions of independent motions, and an integration process that smoothes small, noisy, local variations in velocity and connects the pieces of local motion associated with the same moving object. These two competing processes are nonetheless intimately connected, and it is a major challenge to understand how the visual motion system decides which local motion signals should be pooled together to obtain a precise unitary coherent motion percept, and which to keep segregated to detect motion-defined object boundaries, transpar-

---

* Corresponding author. Tel.: + 33-491-164314; fax: + 33-491-774969.

E-mail address: masson@lnf.cnrs-mrs.fr (G.S. Masson).

ency, or motion-in-depth. Previous psychophysical and computational studies have pointed out that the answer to this question depends on a number of factors; there are interactions in both the spatial and velocity domains, with segmentation performance dependent on both the vector difference between motion signals as well as their spatial distributions. The goal of the present study is to examine the spatial interactions underlying motion segmentation from speed cues alone, by examining segmentation performance while manipulating the local spatial structure of both overlapping and non-overlapping stimuli.

Motion segmentation of stimuli with overlapping (i.e. motion transparency) and non-overlapping (i.e. motion boundary) velocity distributions has been extensively investigated, although mainly in separate studies. A striking contrast between these sets of results is the apparent difference in perceptual sensitivity. Thresholds for detecting the presence of two non-overlapping populations of dots moving in different directions or speeds are relatively low, about 2° for direction and about 5–10% for speed (Nakayama, 1981; Nakayama & Tyler, 1981; Nakayama, Silverman, MacLeod, & Mulligan, 1985; Golomb, Andersen, Nakayama, MacLeod, & Wong, 1985; Snowden, 1992; Sachtler & Zaidi, 1995). However, detecting two transparent surfaces requires larger differences in direction or speed. Specifically, transparency is not perceived unless the directions of motion of the two populations of dots differ by more than about 30–40° (Mather & Moulden, 1980; van Doorn & Koenderink, 1983; Wishart & Braddick, 1997; Smith, Curran, & Braddick, 1999) or the speeds differ by more than about 20–30% (Masson, Mestre, & Stone, 1999). These elevated thresholds therefore suggest that there is some penalty associated with transparency, or some benefit associated with the presence of large regions of homogenous motion or of motion boundaries.

Previous studies have also pointed out that motion segmentation is affected by local spatial interactions. One approach has recognized that a single motion boundary splitting an image versus a fully transparent motion can be considered as the two extremes of a continuum across spatial scale, with the former viewed as extremely coarse corrugation and the latter as infinitely fine corrugation. In their seminal work, van Doorn and Koenderink (1982a,b) investigated the signal-to-noise ratio needed to detect spatial corrugation defined by oppositely directed motion, as the spatial frequency of the square-wave corrugation varied from coarse to fine. They reported that at low spatial frequencies of corrugation (i.e. large bar widths) corrugation was perceived, while at high spatial frequencies (bar widths below ∼0.4°), transparency was perceived. A second approach used to investigate spatial interactions was introduced by Qian, Andersen, and Adelson

(1994a,b). By balancing local motion signals of opposite directions (i.e. confining pairs of dots moving in opposite direction to remain within a small region), they blocked the percept of transparency and instead produced one of flicker, with no net motion. They reported that the critical pairing distance (i.e. the distance between dots moving in opposite directions at which motion transparency is eliminated) was ∼0.4°, similar to the distance at which the perception of corrugated patterns switches from corrugation to transparency (van Doorn & Koenderink, 1982a,b; Watson & Eckert, 1994). They concluded that the perception of motion transparency requires locally unbalanced motion signals, i.e. local regions with a net motion signal in one direction. These two sets of results suggest that a mechanism with a small spatial scale constrains early motion segregation from direction cues.

In the present study, using both locally paired and corrugated stimuli, we determined the critical spatial scale for motion segregation from speed cues. In a recent study (Masson et al., 1999), we defined the smallest speed difference that supports reliable segmentation of moving random-dot stimuli using speed cues alone as the 'speed-segmentation threshold'. We used this threshold as an objective measure of the motion processing involved in speed-based segmentation. We then determined that the speed tuning of this process was constrained to speeds slower than ∼16°/s, consistent with the rather low high-speed limit of the speed tuning of neurons in primary visual cortex (V1). Here, we have extended those results by investigating the spatial scale of the speed-based segmentation mechanism. Specifically, we measured the dependence of speed-segmentation thresholds on the spatial distribution of the motion vectors in corrugated random-dot stimuli, by varying the corrugation spatial frequency, dot density, and eccentricity, under both paired and unpaired conditions. Preliminary results have been reported elsewhere (Mestre & Masson, 1998; Masson & Mestre, 1998).

2. General methods

In all of the experiments described below, using a two-interval forced-choice (2IFC) paradigm, we measured the minimum speed differences necessary to make accurate judgments about moving random-dot stimuli containing subpopulations of dots moving at different speeds, albeit in the same direction. A 'test' interval always contained a corrugated pattern of moving random dots with alternating horizontal bars containing dots moving at two different speeds (Fig. 1a). A 'reference' interval also contained a patch of moving random dots, but its exact configuration depended on the experiment. Observers were asked to indicate which of the

two intervals was the test. No feedback was ever provided. The specific methods for each experiment describe how and why a number of parameters were changed, including the density, mean speed, eccentricity of the dots.

For both the test and reference intervals, the stimulus was a $7° \times 7°$ square patch of moving random dots. Unless stated otherwise (i.e. in the pairing experiment), dots were randomly distributed in the horizontal dimension. In the vertical dimension, to maximize dot homogeneity, we divided the number of dots by the number of bars in the display and randomly placed that (equal) number of dots within each bar. We used multiple bar widths, ranging from $3.5°$ (i.e. 2 bars) to $0.05°$ (i.e. 128 bars). Given that the smallest bar width corresponded to a single display scan line, in that one particular case, all of the dot trajectories within a bar actually overlapped.

Each dot extended 2 pixels horizontally and 1 pixel vertically. Given the spatio-temporal resolution of our video projection system, the smallest speed that could be produced by shifting one pixel on every frame was $3.8°/s$. To produce smaller speed differences, we used a sub-pixel animation procedure along the horizontal axis (Georgeson, Freeman, & Scott-Samuel, 1996). The smallest difference in speed that could be generated in this way was $0.025°/s$, allowing variation in speed down to 5% for the lowest mean reference speed used ($1°/s$). We used a PEST algorithm (Taylor & Creelman, 1967)

to 'staircase' the speed difference to that yielding 75% correct performance. The smallest PEST step size was of 5% ($\pm$ 2.5%). To reduce motion adaptation effects, the direction of motion was randomly leftward or rightward on a trial-by-trial basis. To obtain a stable threshold measure, observers performed up to five repeated runs of 70 trials for each condition. We fitted individual psychometric data with a Weibull function using a Simplex algorithm (Matlab®) to determine the speed difference (expressed as a percentage of the constant mean speed) yielding 75% correct performance.

Visual sequences were generated on a Silicon Graphics workstation (Octane MXE, 2xR10000) using OpenGL graphics primitives. Each dot trajectory was pre-calculated, and a 'wrap-around' procedure was used to keep the dot density constant throughout the presentation interval. The trajectories were then stored on disk for later display. Six movies were generated for each condition (different instances of random dots), which were interleaved during each session. Random dots of luminance 25 cd/m² were back-projected onto a large tangent screen at a refresh rate of 76 Hz, using a RGB video projector (Electrohome Marquee 7000). A chin and forehead rest stabilized the observer's head; the image was at eye level and was viewed binocularly from a distance of 1 m. The display resolution was 1280×1024 pixels, and at the chosen viewing distance, each pixel subtended a visual angle of $0.055°$. The screen background and experimental room were dark (< 0.01 cd/m²). The randomized presentation of stimuli as well as the recording of the perceptual responses (using response keys) was controlled on-line by a PC (HP 486) connected to the graphics station via a serial RS232 interface. The square target stimulus always first appeared stationary for a random period of time (300–700 ms) and was then set in motion for 200 ms (15 frames). A blank inter-stimulus interval of 500 ms was followed by a second stimulus interval of 200 ms. To minimize reflex tracking eye movements, a blue fixation cross ($1° \times 1°$, 5 cd/m²) was displayed at the center of the stimulus. The large screen display allowed both central and peripheral presentation, with observers looking straight ahead.
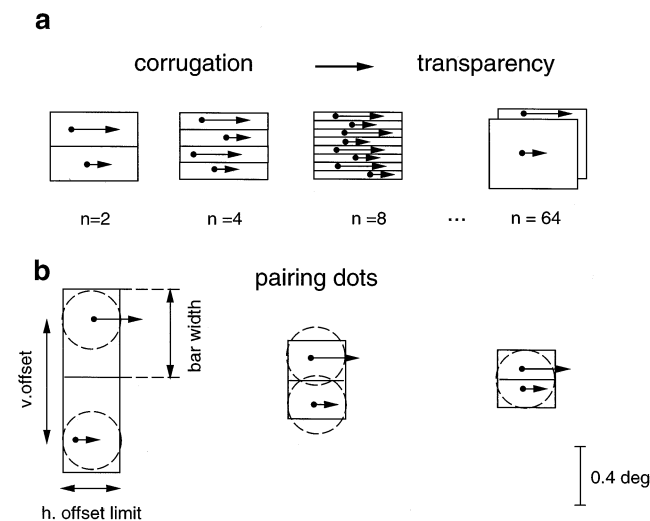
Fig. 1. Schematics of our corrugated stimuli. (a) Each display is divided into an even number of horizontal bars of equal width. One speed (V_1) is attributed to the odd bars, while a second speed (V_2) is attributed to the even bars. The speed difference is manipulated to determine the speed-segmentation threshold as a function of bar width. (b) This panel depicts the progressive effect of dot pairing (with its jittered small horizontal offset) as the stimulus bar width (to which the vertical offset is linked) decreases. When the vertical offset becomes smaller than the local pairing area, the dots become locally paired.

3. Experiments

3.1. Experiment 1: Speed-based segmentation of corrugated patterns and its associated percepts

In this initial set of experiments, we examined the spatial scale of motion segmentation using two different tasks. In a first experiment using a global-motion discrimination task, we measured the speed difference necessary to support accurate visual motion-based segmentation of a corrugated display (Fig. 1a) as a func-

tion of the bar width. However, as has been pointed out previously (van Doorn & Koenderink, 1982a,b), corrugated stimuli can elicit different spatial percepts depending on the velocity difference between the bars and on the bar width. For our stimuli (i.e. random dots moving in the same direction in a corrugated pattern defined by alternating bars containing two different speeds), below some threshold speed-difference, the coherent motion of a single population of moving dots is observed. Above threshold, observers subjectively reported seeing a corrugated pattern with alternating bars moving at different speeds at large bar widths, and two transparent surfaces moving at different speeds at small bar widths. In a second experiment using a spatial-discrimination task, to quantify the above subjective impressions, we directly measured the bar width at which this perceptual transition occurs.

3.1.1. Specific methods

These initial experiments were performed on two authors (D.M. & G.M.). Both had normal or corrected-to-normal vision. The stimuli were centered on the fovea (fixation point) and had a mean dot speed of 8°/s and density of 10.56 dots/deg^2.

3.1.1.1. Speed-segmentation task.
Using a 2IFC task previously described in Masson et al. (1999), observers were asked to detect in which of two sequentially presented temporal intervals two and only two moving speeds were present (a motion judgment). In the test interval, half of the dots moved at a speed of $V_1 = (V_{mean} + \Delta V/2)$ in the even-numbered bars, while the other half moved at $V_2 = (V_{mean} - \Delta V/2)$ in the odd-numbered bars, with ΔV, the speed difference, being tested on a given trial. To prevent observers from basing their perceptual judgments simply on the detection of any local speed difference and bypassing a global segmentation process, the reference interval consisted of subpopulations of randomly positioned dots moving at five different speeds, evenly distributed between V_1 and V_2. Both intervals always had the same mean speed (V_{mean}). We defined the 75% point of the best-fitting Weibull function to the psychometric data as the speed-segmentation threshold.

3.1.1.2. Corrugation-perception task.
The procedures were identical to those for the segmentation task above, except that (1) although the reference interval contained two subpopulations of dots with the same two speeds as the test, the dot locations were fully spatially randomized (i.e. above threshold, this stimulus is perceived as two transparent sheets of dots), and (2) observers were asked to determine which of the two temporal intervals was corrugated (a spatial judgment). We defined the 75% point of the best-fitting Weibull function to the psychometric data as the corrugation-detection threshold.

3.1.2. Results

Our first finding is that speed-segmentation varies systematically with bar width. Fig. 2 plots the speed-segmentation thresholds for both observers (Fig. 2ab, closed symbols). Note that the curves are sigmoid (S-shaped) with lower thresholds at larger bar widths (on the left-hand side of the graphs), higher thresholds at smaller bar widths, and an inflection at the mid-range bar widths. Fig. 2c plots the average thresholds ($\pm$ S.D.) across observers. On average, the speed-segmentation thresholds increased from $\sim 17\%$ up to $\sim 45\%$ as the bar width decreased from 3.2° to 0.1°. To estimate the inflection point, we fit each individual curve with the Naka–Rushton function (Naka & Rushton, 1966) to determine the bar width at which the speed-segmentation threshold reaches 50% of its maximum, Thr50. For the two observers, Thr50 was 0.39° and 0.41°.

Our second finding is that the transition between low and high speed-segmentation thresholds corresponds well with the previously described perceptual transition between corrugation and transparency (van Doorn & Koenderink, 1982a,b). Fig. 2 plots the corrugation-detection thresholds for both observers (Fig. 2ab, open symbols). At large bar widths, the corrugation-detection thresholds superimpose on the speed-segmentation thresholds (i.e. segmentation and corrugation perception require the same minimum speed difference), while at small bar widths, the corrugation-detection threshold increases beyond the segmentation threshold and ultimately blows up as corrugation perception becomes impossible (i.e. transparency and corrugation are no longer distinguishable). Fig. 2c again plots the average thresholds ($\pm$ S.D.) across observers. On average, a significant difference between the two thresholds first occurs at a bar width of 0.2° (*t*-test, $P < 0.02$), which is also the value at which the high segmentation-threshold plateau appears. By comparing the two threshold curves, we can functionally divide the stimulus space into three regions yielding three different percepts: transparent, corrugated, and coherent (i.e. unsegmented) motion (Fig. 2c).

3.2. Experiment 2: Effect of dot pairing and eccentricity

In a second set of experiments, we further investigated the spatial scale of the interactions between local motion signals underlying motion segmentation by measuring the effects of pairing and eccentricity on the relationship between speed-segmentation threshold and bar width (Fig. 1b).

3.2.1. Specific methods

One naïve observer (Y.R.) and two authors (G.M., D.M.) participated in Experiment 2. All had normal or
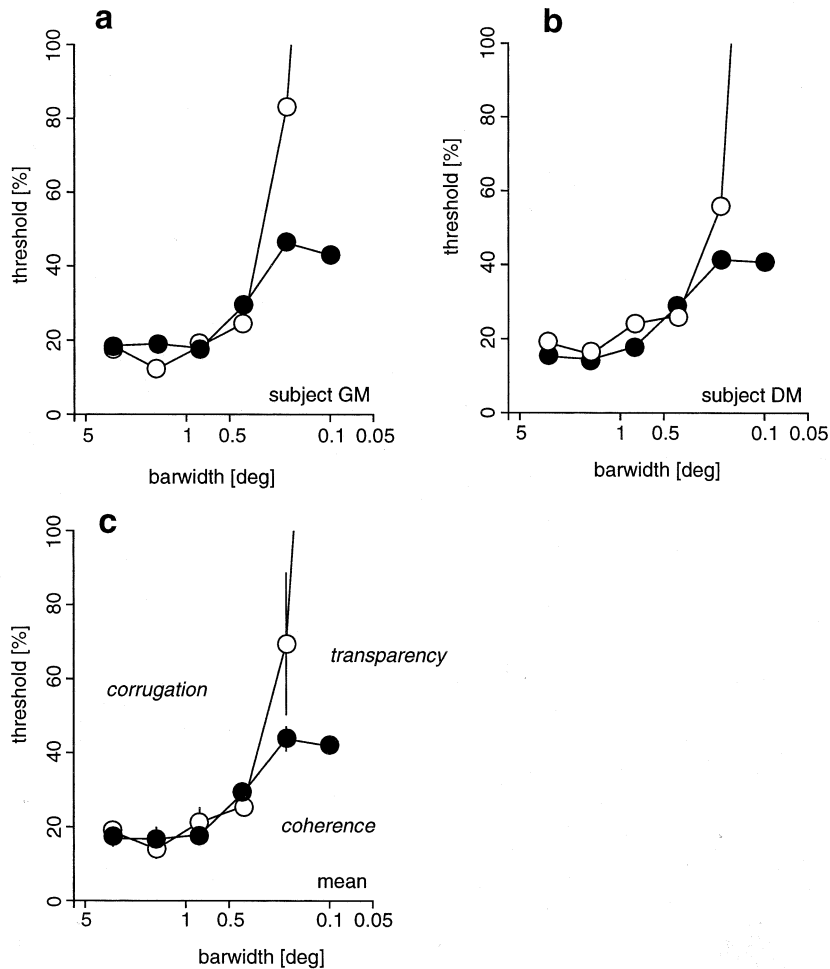
Fig. 2. Motion segmentation of corrugated stimuli and the associated spatial percepts. Individual (a,b) and average (± S.D. across observers) (c) thresholds. The speed-segmentation thresholds as a function of bar width are plotted as closed symbols. For comparison, corrugation-detection thresholds are plotted as open symbols. Note that these results divide the parameter space into three perceptually distinct zones: corrugation, transparency, and coherence.

corrected-to-normal vision. The naïve observer was familiar with visual psychophysical tasks, but was unaware of the purpose of the experiments. The methods were as for the speed-segmentation task described in Experiment 1, except for the following.

We measured speed-segmentation thresholds under two conditions, paired and unpaired. In both the paired and unpaired conditions, the reference stimulus was physically corrugated (although never perceived as such); dots moving at speeds of V_1, V_{mean} and $(V_1 + V_{mean})/2$ were assigned to the even bars, while dots moving at V_2, V_{mean} and $(V_2 + V_{mean})/2$ were assigned to the odd bars.[1] In the paired condition, each dot in an even bar was associated (i.e. paired) with a dot in the

adjacent odd bar (Fig. 1b). Once the first dot was randomly placed, the second dot was placed in such a way that its horizontal offset from the first dot was always less than or equal to 0.22° (4 pixels) throughout the presentation interval (200 ms). A small amount of random jitter was added to the horizontal offset to prevent the perception of a regular pattern. In the vertical dimension, the distance between the two dots was exactly equal to the bar width. Three mean eccentricities used were 0° (extending 3.5° on either side of a central fixation point), 7° (3.5–10.5°), and 14° (10.5–17.5°), tested in separate blocks. For each eccentricity, speed-segmentation thresholds were measured for each bar width under the two pairing conditions. For the eccentric conditions, the stimuli appeared randomly on either the right or the left side of the central fixation target. Because of the severe constraints imposed by pairing (i.e. needing to keep the horizontal position of the two paired points within 0.2° for 200 ms), we used

[1] The similarity of the results of Experiments 1 and 2 shows that the exact spatial configuration used in the reference interval was not critical, as both reference stimuli used were perceived as transparent within the speed-difference range examined in our experiments.

a mean speed of only 1°/s, even though we have shown previously that this speed is well below optimal for this task (Masson et al., 1999). We also used a low dot density (2.56 dots/deg²) to minimize the random 'pairing' caused by the fortuitous proximity of two dots moving at different speeds. To examine the effect of eccentricity alone without the constraints imposed by pairing, we performed a second experiment on two authors using a higher dot density (512 dots; 10.56

dots/deg²), four mean eccentricities (0, 3.5, 7, and 14°), and a higher mean dot speed of 8°/s.

3.2.2. Results

Fig. 3a, d, g plot the speed-segmentation threshold of all three observers as a function of bar width under foveal viewing. Note that, at large bar widths, observers show similar performance in the paired and unpaired conditions. However, a large deviation develops at
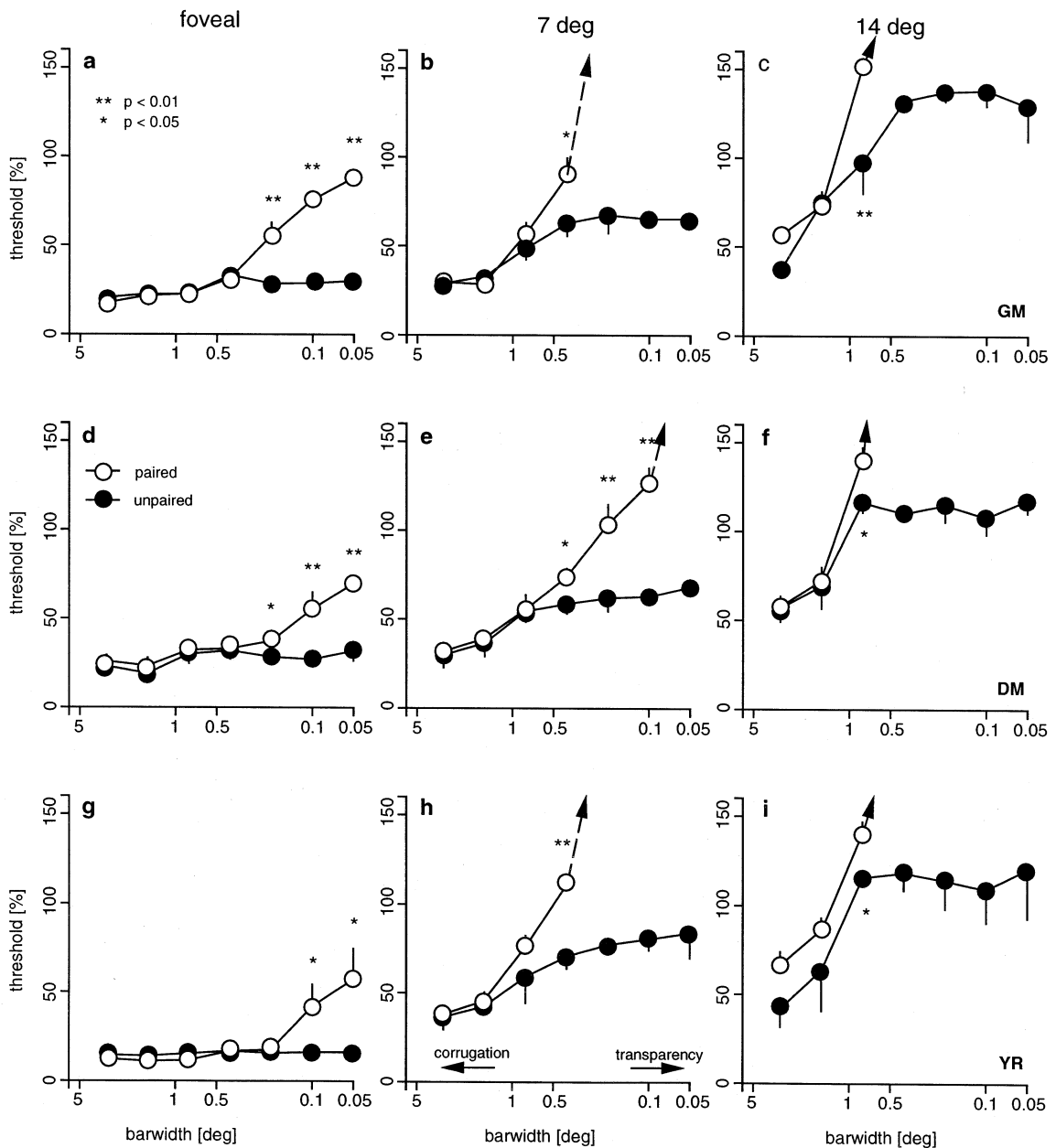
Fig. 3. Effect of pairing on individual speed-segmentation performance. The mean (± S.D. across runs) speed-segmentation thresholds are plotted as a function of bar width, for each observer (rows) and three stimulus eccentricities (columns). The closed and open symbols represent the unpaired and paired conditions, respectively. The broken arrows indicate that, for conditions in which dots with different speeds were locally paired, no threshold was measurable at small bar widths within the speed-difference range used. For each observer, asterisks indicate bar widths for which there is a significant threshold difference between the paired and unpaired conditions (Student t-test, *P < 0.05; or **P < 0.01, Bonferroni-corrected).
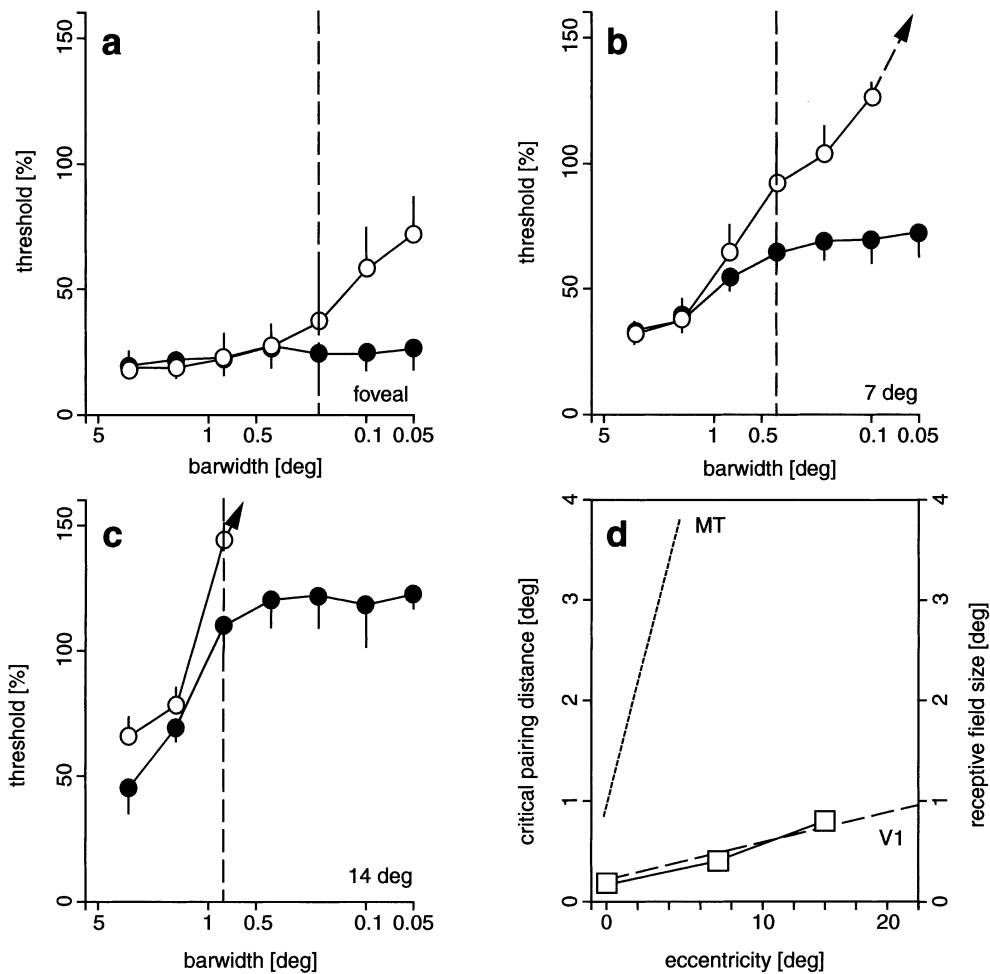
Fig. 4. Average effect of pairing on speed segmentation. (a–c) The average ($\pm$ S.D. across observers) speed-segmentation threshold is plotted as a function of bar width, for three stimulus eccentricities. The vertical dotted lines indicate the highest average bar width (defined as the critical pairing distance) for which a significant difference between paired and unpaired condition was found. (d) The average critical pairing distance is plotted as a function of eccentricity. The dashed lines illustrate the relationships between the receptive field sizes of V1 and MT neurons and eccentricity, respectively (from Dow et al., 1981 and Albright & Desimone, 1987).

smaller bar widths; in the unpaired condition, speed-segmentation thresholds increase only slightly, while in the paired condition, performance decreases dramatically (thresholds increase sharply). The reason that pairing has no effect on speed-segmentation thresholds at large bar widths is presumably due to the large vertical offset between the 'paired' dots at low spatial frequencies of corrugation (see, Fig. 1b). However, pairing has profound effects at small bar widths, more specifically when the pair's vertical offset goes below some critical value. For foveal viewing, this 'critical pairing distance' (the largest distance that for which there is a significant difference between the paired and unpaired thresholds) is between 0.1 and 0.2°. The performance pattern is reflected even more clearly in plots of speed-segmentation threshold averaged across observers (Fig. 4a). The clear deviation of the paired from the unpaired thresholds indicates that pairing blocks the speed-segmentation process when all pairs of dots moving at different speeds

co-exist within an integration region smaller than about 0.2°.

If this critical pairing distance is related to a constraint in an early visual mechanism, it should increase slowly with eccentricity, as do the receptive fields within early visual cortical areas. Fig. 3b, e, h plot the average speed-segmentation thresholds at 7° of eccentricity and Fig. 3c, f, i those at 14° of eccentricity, for all three observers. As eccentricity increases, the paired and unpaired curves begin to diverge at larger bar widths. The vertical dashed line in Fig. 4a, b, c indicates the critical pairing distance. They shift leftward, from 0.2 to 0.8°, as eccentricity increases from 0° to 14° (Fig. 4d). This relationship can be fit by a line of slope 0.045 with an intercept of 0.14° ($r = 0.99$). Interestingly, this trend is quite similar to that reported by Dow, Snyder, Vautin, and Bauer (1981) for the change in receptive field size of macaque V1 neurons as a function of eccentricity (dashed line in Fig. 4d). They found a slope of 0.044 and an intercept of 0.22°. For comparison, we also plotted thear

linear relationship between receptive field size and eccentricity for primate MT neurons (dotted line defined by a slope of 1.04 and intercept of 0.61; Albright & Desimone, 1987). The observed relationship between critical pairing distance and eccentricity is appropriate for a mechanism with a V1-like receptive field size that clearly operates at a much finer scale than that of MT receptive fields.

In Figs. 3 and 4, it is clear that increasing the stimulus eccentricity raised the overall speed-segmentation thresholds, even for the unpaired condition, and changed the shape of the curves. We further investigated this point by measuring the relationship between the unpaired speed-segmentation thresholds and bar width at four different eccentricities using a higher dot density and dot speed, as we were no longer constrained by the pairing process.

The results for the two observers are shown in Fig. 5a, b. For foveal presentation (solid circles), decreasing bar width increases speed-segmentation thresholds up to a plateau around 30%. At the higher speed and dot density, the curves became more clearly S-shaped with a pronounced inflection point (compare Figs. 2 and 5 with Figs. 3 and 4). Three major eccentricity effects are apparent. Firstly, thresholds increased monotonically with eccentricity, for all bar widths. For both observers, the mean threshold, averaged across bar widths, increased pseudo-linearly with eccentricity (Fig. 5c, d insets). Averaged over observers, asymptotic values for the smallest bar width increased from $31.4 \pm 0.3\%$ in the fovea to about $74.4 \pm 12.7\%$ at 14° eccentricity. For the largest bar width, the increase was from $15.9 \pm 3.0\%$ to $32.9 \pm 4.7\%$. Secondly, the curves became more S-shaped with increasing eccentricity, i.e. the difference between the lowest and the highest thresholds along the curves increased. This effect is made clearer if the thresholds are 'adjusted' by subtraction of the mean threshold across widths (Fig. 5c, d). This adjustment helps separate the overall effect of stimulus eccentricity (e.g. McKee & Nakayama, 1984; Donadio, Mestre, & Masson, 1998) from the concomitant effect of changing the spatial scale. More specifically, increasing eccentric-
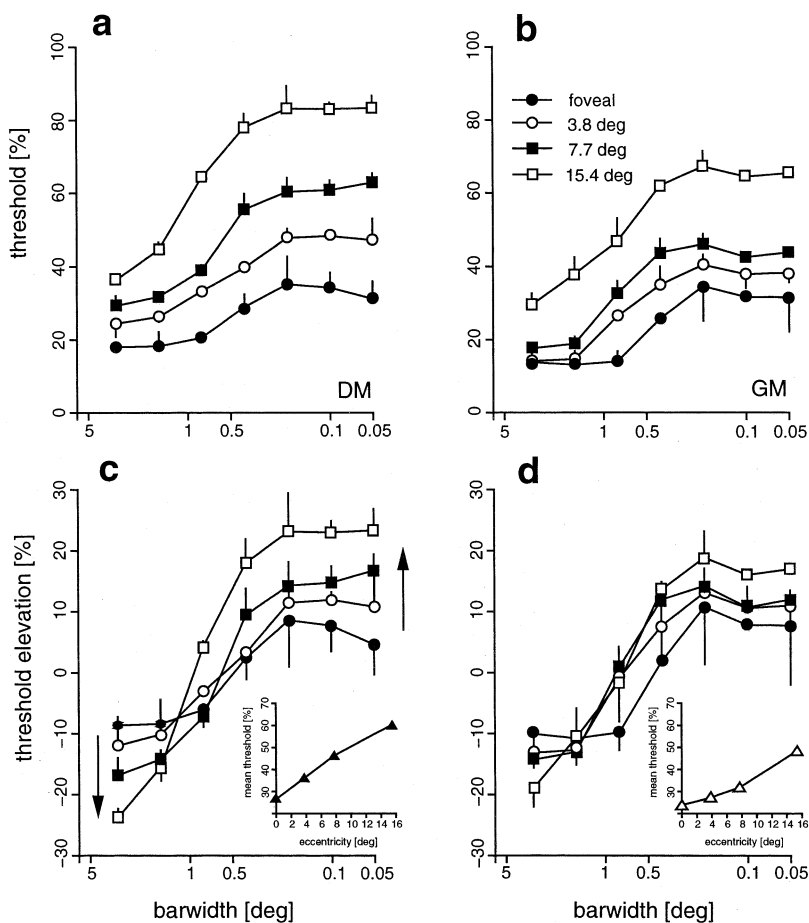
Fig. 5. Effect of stimulus eccentricity on speed segmentation. (a, b) The speed-segmentation thresholds are plotted as a function of bar width for four different eccentricities. (c, d) The thresholds are replotted after subtraction of the mean thresholds across all bar widths, for each observer. The S-shaped curves become sharper as eccentricity increases; relative thresholds decrease for large bar widths but increase for small bar width (arrows). The mean speed-segmentation thresholds are plotted as a function of eccentricity in the inset graphs.

ity lowered the adjusted thresholds for large bar widths, but increased them for small bar widths (as indicated by the arrows in Fig. 5c), making the sigmoid nature of the curve sharper. Thirdly, increasing eccentricity shifted the inflection point of the threshold curves towards larger bar widths. Averaged across observers ($\pm$ S.D.), the best-fitting Thr_{50} increased from $0.48 \pm 0.03°$ in foveal vision to $0.98 \pm 0.10°$ at $14°$ of eccentricity. A significant linear relationship between the inflection point and eccentricity was found with a slope of 0.03 and an intercept of $0.57°$ ($r = 0.82$). The slope is again similar to that for V1 neurons, but much lower than that for MT neurons.

3.3. Experiment 3: Effect of dot density

The results of Experiments 1 and 2 indicate that speed segmentation is constrained by a mechanism that operates over a restricted spatial extent. Forcing pairs of different motion vectors to fall within the same small spatial area revealed this local pooling zone. However, in general, for all transparent displays consisting of two populations of dots randomly distributed over space, there is always the possibility that the pairing two dots of different speeds occurs by chance transiently at a given location and time. Furthermore, the probability of such chance pairings increases with dot density and with the spatial frequency of the corrugation. To examine this stochastic phenomenon, we measured the effect of dot density on the relationship between speed-segmentation threshold and bar width.

3.3.1. Specific methods

One naïve observer (G.D.) and two authors (G.M., D.M.) participated in this experiment. All had normal or corrected-to-normal vision. The naïve observer was familiar with visual psychophysical tasks, but was unaware of the purpose of this experiment.

The methods were identical to those used in Experiment 2, except that we used only unpaired dots, foveal viewing, and the mean dot speed was $8°/s$. Furthermore, we tested observers with three-dot dot densities, 2.56, 10.34 and 41.32 dots/deg^2 (corresponding to 128, 512 and 2048 dots, respectively), in separate blocks.

3.3.2. Results

Fig. 6 plots the speed-segmentation thresholds of the three observers as a function of bar width (Fig. 6a, b, c) as well as the average across observers (Fig. 6d). For all observers, as the dot density increased, the S-shaped nature of the curves became more pronounced. Specifically, at the largest bar width ($3.2°$), increasing the dot density from 2.56 to 41.32 dot/deg^2 decreased the average threshold from $15.4 \pm 4.1\%$ to $7.3 \pm 0.8\%$. However, at the smallest bar width ($0.05°$), increasing dot density across the same range increased threshold,

from $19.8 \pm 2.4\%$ to $40.1 \pm 4.2\%$. Note, however, that the three S-shaped curves intersect at nearly the same point. No significant change in the Thr_{50} value was observed as dot density increased from 2.56 to 41.32 dots/deg^2. Averaged across observers ($\pm$ S.D.), the Thr_{50} was 0.46 ± 0.01, 0.47 ± 0.08, and 0.36 ± 0.06, for the three increasing dot densities. A linear regression through the individual data indicated a flat relationship between Thr_{50} and dot density (intercept: 0.41, slope: -0.012, $r = 0.71$). This result suggests that the spatial scale of the underlying mechanism was unaffected by changing the dot density.

4. General discussion

Previous studies on motion segmentation have shown that motion segmentation depends strongly on the spatial distribution of dots in the visual field, as demonstrated by experimental manipulations of dot pairing, bar width, dot density, and eccentricity (e.g. Nakayama, 1981; van Doorn & Koenderink, 1982a,b; Qian et al., 1994a; Sachtler & Zaidi, 1995; Watson & Eckert, 1994; Wishart & Braddick, 1997). These earlier studies, however, presented motion in different directions and/or used a criterion-dependent spatial judgment. In the present study, we investigated the spatial scale of motion segregation using primarily a 2IFC global-motion task, the discrimination of two unidirectional random-dot motion patterns, distinguishable only by their global distributions of speeds. We thus avoided the potentially confounding issues of motion opponency and of simply using a local velocity difference alone to perform the task.

This study has three main findings. First, speed-based segmentation requires a larger speed difference to support reliable performance with transparent displays created by the simultaneous presentation of two overlapping (or nearly so) populations of random dots moving at different speeds than with coarsely corrugated displays created using non-overlapping populations of random dots (this study) or than for the simple discrimination of the same two speeds presented in successive random-dot displays (Masson et al., 1999). Consistent with our earlier study using spatially uniform, large-field, random-dot displays, in foveal vision, speed-segmentation thresholds ranged between 30 and 40% for transparent displays (i.e. those with the smallest bar width) with a similar mean speed, dot density and stimulus duration (see for comparison Fig. 2, Masson et al., 1999). The present data extend this earlier result to reveal that thresholds decrease along an S-shaped curve as the bar width increases, with a lower asymptote in foveal vision between 15% and 20% for displays with the coarsest corrugation (i.e. those with the largest bar width). The critical spatial scale for
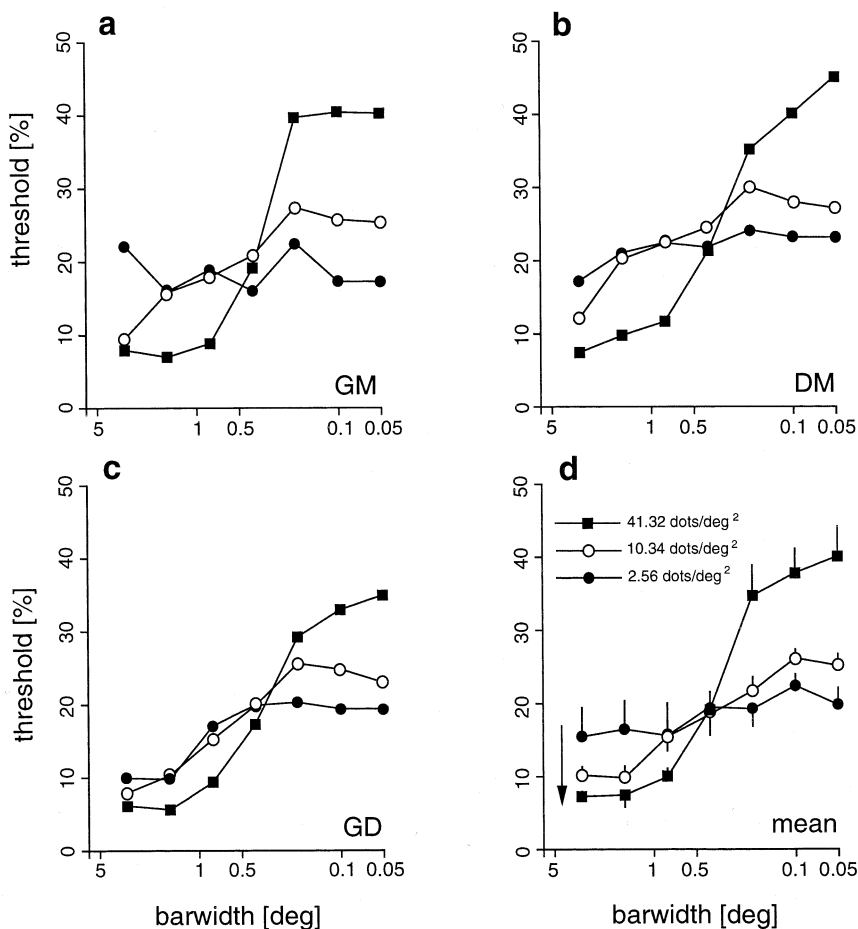
Fig. 6. Effect of dot density on speed segmentation. (a–c) The speed segmentation thresholds for three different dot densities are plotted as a function of bar width for each observer. (d) The average (± S.D. across observers) speed-segmentation thresholds are plotted as a function of bar width, for three dot densities. As dot density increases, the threshold increases (decreases) for small (large) bar widths (see arrows).

speed segmentation occurs at a bar width of $\sim 0.2°$, as demonstrated by the pairing experiment. Below this spatial scale, with unpaired displays, motion transparency is perceived, and observers were no longer able to perceive corrugation regardless of the speed difference (Fig. 3). The Thr_{50} point of the S-shaped speed segmentation curves was found to be $\sim 0.4°$ in foveal vision, which largely coincides with the spatial scale at which the perceptual transition between transparency and corrugation occurs. Corrugated and transparent displays were not distinguishable, independent of the speed difference, for bar width of $\sim 0.2°$, a value that is similar to the critical pairing distance. Second, we found two effects of eccentricity. Increasing the stimulus eccentricity increased the speed-segmentation threshold at all bar widths. In addition, the critical spatial scale, as reflected in the critical pairing distance and the Thr_{50} point, increases slowly with stimulus eccentricity and does so in a manner quantitatively similar to V1 receptive-field sizes in primates (Dow et al., 1981). Third, we found a dramatic effect of dot density. The 'sharpness'

of the S-shaped curve increases as dot density increases (speed-segmentation thresholds become higher for transparent motion, lower for corrugated motion), while the spatial properties of the S-shape curves (i.e. its inflection point) remain unchanged.

4.1. Spatial characteristics of speed segmentation

Several examples of the detrimental effects of one motion signal on the detection/discrimination of a second, transparently displayed, motion signal have been reported using direction differences (e.g. Mather & Moulden, 1980; Snowden, 1989; Wishart & Braddick, 1997; Smith et al., 1999; Curran & Braddick, 2000). The poorer performances in direction-based and now speed-based segmentation suggest the existence of inhibitory spatial interactions within and/or across the receptive fields of cortical neurons, driven by two proximate yet disparate velocity vectors. Several recent psychophysical and neurophysiological studies point out the need to understand the nature and spatial scales of

these local interactions (see Braddick, 1997 for a re-view). However, because different spatial distributions of dots can lead to qualitatively different spatial per-cepts, it is preferable to use a non-spatial task, so that performance is not contaminated by any potential per-ceptually driven shift in spatial criteria. Therefore, we designed a global-motion segmentation task in which observers were asked to detect which interval contained two, and only two, speeds. Therefore, a simple set of rules such as detecting bimodal subpopulations of re-sponses within a population of speed-tuned motion units is sufficient to perform the task. The observed dependence of threshold on the spatial distribution of the dots provides a robust measure of the spatial inter-actions within the speed-segmentation mechanism.

As found previously for motion-detection thresholds (Nakayama & Tyler, 1981; van Doorn & Koenderink, 1982a,b), decreasing the bar width of corrugated pat-terns increased the speed-difference threshold for the detection of corrugation. Our results extend this to show that below 0.2°, speed-segmentation thresholds hit a plateau around 40%, a value close to those found previously with fully randomized random-dot patterns (Masson et al., 1999). We found an S-shaped relation-ship between the performance of the speed-segmenta-tion mechanism and the spatial distribution of dots, indicating that speed segmentation is indeed con-strained by spatial interactions. We further demon-strated that, above threshold, different bar-width conditions resulted in different motion percepts; for large bar widths, non-overlapping bars of alternating speeds are perceived, while for small bar widths, over-lapping moving surfaces are perceived.

The S-shaped relationship linking speed segmenta-tion and the spatial distribution of moving dots was affected by several factors. First, we found that dot pairing within a critical distance produces a sharp increase in the speed-segmentation threshold. Speed segmentation is blocked with a critical pairing distance of $\sim 0.2°$ in central vision, a value similar to that found by Wishart and Braddick (1997) for motion segmenta-tion from direction cues and by Qian et al. (1994a) for opponent motion. Interestingly, this value is nearly the same as the bar width at which the S-shaped speed-seg-mentation threshold curves reach a plateau, and at which corrugation perception is no longer possible (and instead transparency is perceived). We also found that both the critical pairing distance and the inflection point scale quasi-linearly with eccentricity. Moreover, when eccentricity is increased, not only do speed-seg-mentation thresholds increase, but also the S-shaped threshold functions are transformed. In addition to a general performance decrement with peripheral view-ing, as expected for motion perception (e.g. McKee & Nakayama, 1984), which can account for the overall upward shift of the curves, the change in the shape of

the curves results in a shift of the Thr_{50} point towards larger bar widths, and presumably of the associated transition between corrugation and transparency. This shift is exactly what one would expect from an increase in the spatial scale of the underlying neuronal mecha-nism with eccentricity.

These results are all consistent with the view that a local pooling mechanism constrains motion segmenta-tion. Local pairing is assumed to force the pooling of the two different velocity signals (Qian et al., 1994a, b; Wishart & Braddick, 1997), which then blocks motion segmentation. A similar mechanism has been postulated to explain why motion detection performance increased as the corrugation frequency of a motion-shearing dis-play decreased (Nakayama & Tyler, 1981). This view is also consistent with the results of Nawrot and Sekuler (1990), who manipulated the bar width of a corrugated pattern made of alternating bars of moving dots and dynamic noise. They found that the motion of the alternate motion bars captures the dynamic noise at small bar widths, but induces illusory motion of the dynamic noise in the opposite direction at large bar widths. They suggested that a local pooling mechanism, with an inhibitory surround, can explain the observed motion-capture phenomenon.

Local pooling is also consistent with our dot-density findings. When dot density was manipulated in central vision, the inflection point of the S-shaped threshold functions remained unchanged, reflecting the fact that dot density has no effect on the spatial scale of the segmentation process. However, as dot density in-creases, the probability of cooperative interactions be-tween identical motion signals within each bar and for inhibitory interactions between disparate motion signals between adjacent bars both increase. For large bar-widths (corrugated patterns), speed-segmentation thresholds decrease as dot density increases. The strengthening of the speed estimate for each bar in-creases with increasing dot density as cooperation ap-pears to dominate. For small bar widths (transparent patterns), thresholds increase as dot density increases. The probability that two different speeds fall into a single local pooling region increases with increased density, as interference appears to dominate.

4.2. A simple stochastic simulation of putative spatial interactions underlying segmentation

In an attempt to reconcile all of our seemingly dis-parate results within the context of a single postulated local motion pooling mechanism, we performed a set of simple stochastic simulations, which qualitatively repli-cated our main experimental findings (Fig. 7). The simulation assumes that a local pooling unit (of fixed size at a given eccentricity) integrates motion signals

over a small portion of the visual field and limits segmentation performance. It also assumes that the size of this unit is linearly related to eccentricity in the same way that primate V1 receptive fields are (Dow et al., 1981), but is unaffected by other stimulus manipulations (dot density, bar width).

It also assumes that two types of interactions within a local unit's 'receptive field' influence its output: cooperation and interference. We then make a number of simplified assumptions about these two phenomena. First, we postulate that interference can only occur along the border between two bars, in a zone defined by the size of the unit receptive field. The probability of interference is defined, within these interference zones, as the probability of having at least one dot in each side of a unit receptive field (with each of the two speeds) straddling a bar border. Second, we postulate that cooperation can only occur elsewhere in the display. We further postulate that, in the cooperation zone, the

probability of cooperation is defined as the probability of having two or more moving dots (with the same speed) within a receptive field. These probabilities depend on the dot density, bar width, and eccentricity. In particular, the proportion of dots falling within interference zones increases (and reciprocally, that in cooperation zones decreases) as bar width decreases and as the unit size increases with eccentricity. We then arbitrarily define threshold elevation to be the simple difference between the cooperation and interference probabilities. These overly simplified assumptions neglect any variability in receptive-field size at a given eccentricity, any potential interaction across local units (either facilitatory or inhibitory), any potential competition between cooperation and interference within a single local unit, any higher-order effects caused by interactions between more than two dots, as well as any integration of motion information across time. Nonetheless, the skeletal mechanism proposed is suffi-
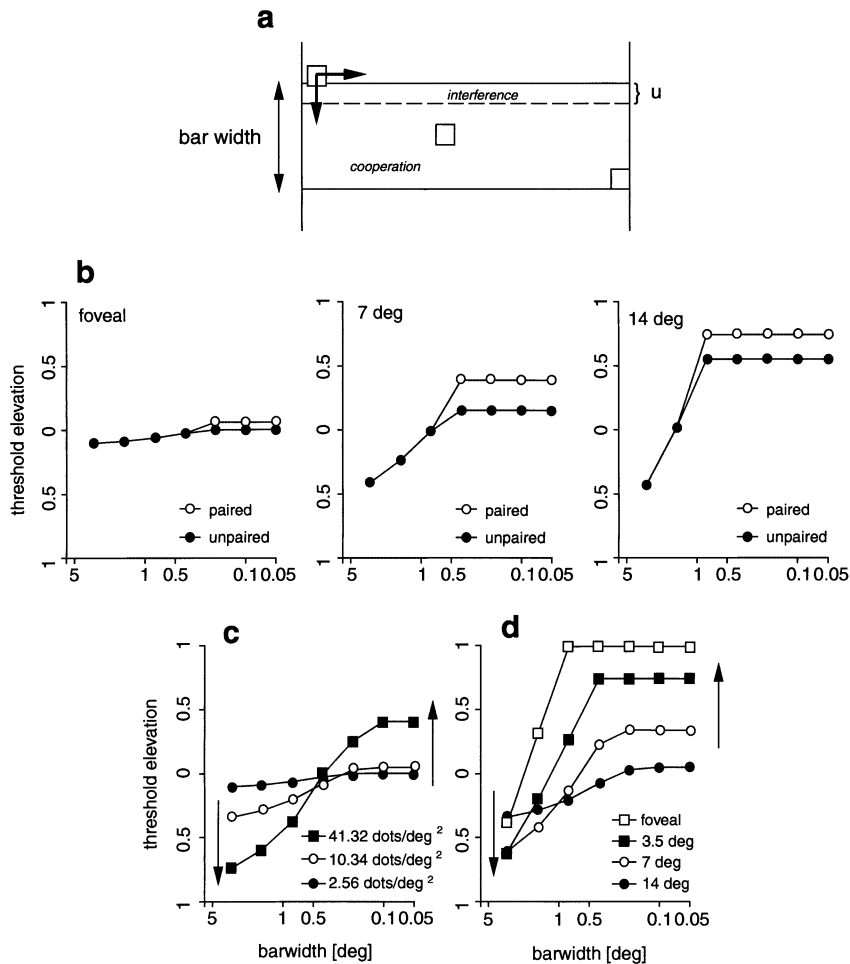
Fig. 7. Simulations of a simple stochastic model (see Appendix A). (a) Illustration of the integration process as the local pooling unit is swept across a bar. (b) The predicted effect of pairing on threshold is plotted as a function of bar width. The open and closed symbols represent the unpaired and paired conditions, respectively. Notice that the plotted threshold elevation is based on probability calculus only and therefore ranges between -1 and $+1$, explaining the saturation discrepancy between Figs. 3 and 7b. (c) The predicted threshold is plotted as function of bar width, for three dot densities in central vision. (d) The predicted threshold is plotted as a function of bar width, for four different eccentricities. Vertical arrows indicate the opposite changes in threshold observed for small and large bar width, when either dot density or eccentricity increases.

cient to capture the essence of the observed trends in speed-segmentation performance.

The simple mechanism (described in more detail in Appendix A) predicts a sigmoidal relationship between speed-segmentation thresholds and bar width (Fig. 7b), as observed (Figs. 3–6), as well as a large increase in threshold at bar widths smaller than the inflection point when dots are systematically paired, as observed (Fig. 3). Furthermore, because the inflection point is associated with the unit size, the mechanism also predicts a lateral shift in the inflection point with eccentricity (Fig. 7d) and an associated shift in the bar width at which thresholds diverge in the paired and unpaired conditions (Fig. 7b) as observed (Fig. 4). Finally, the mechanism also predicts a sharpening of the sigmoidal curve, without any lateral shift of the inflection point with changes in dot density (Fig. 7c) as observed (Fig. 6). These findings strongly support the idea that the constellation of results described above (i.e. the effects of bar width, pairing, eccentricity, and dot density) are linked manifestations of a single constraining pooling mechanism, with a small receptive field that increases slowly with eccentricity.

4.3. Neurophysiological substrates

Visual motion processing is often assumed to be a two-stage mechanism, in which a global motion integration stage follows a local motion detection and measurement stage. These two stages have been attributed to cortical areas MT and V1, respectively (e.g. Movshon, Adelson, Gizzi, & Newsome, 1985; Albright & Stoner, 1995). Within this scheme, it remains unclear where motion segregation (the distinction of multiple velocities) and integration (the grouping of similar velocities) occur. Braddick (1997) suggested that at the core of this problem is a difference in the spatial scale for these two mechanisms. Psychophysically, we found that transition between motion corrugation and motion transparency occurs at around 0.4°, that this transition is associated with an increase speed-segmentation threshold below 0.4°, that pairing blocks motion segmentation for distances below 0.2°, and finally that these spatial parameters scale weakly with eccentricity in a manner similar to that of the receptive-field size of V1 neurons.

Given that the perception of corrugation is possible even at spatial scales much finer that that of MT neurons, the detection of finely spaced alternating motion boundaries is likely supported by neurons in the earlier stages of the motion pathways, perhaps at the level of V1 or V2. Indeed, selectivity for the orientation of motion boundaries has been reported in primate visual areas V2 and even in V1 (e.g. Lamme, van Dijk, & Spekreijse, 1993; Leventhal, Wang, Schmolesky, & Zhou, 1998; Marcar, Raiguel, Xiao, & Orban, 2000). In contrast, studies investigating the role of area MT/V5 in extracting motion boundaries have given inconclusive

results. Lesion studies produced no clear results (Marcar & Cowey, 1992; Lauwers, Saunders, Vogels, Vandenbussche, & Orban, 2000), and Marcar, Raiguel, Xiao, Maes, and Orban (1995) found that neurons in primate visual area MT were unable to encode unambiguously the orientation of kinetic boundaries. In the same vein, human fMRI studies have reported that the neural activity in visual areas V1, V2 or V3 is strongly modulated by the spatial frequency of a corrugated pattern, while activity in area MT is only weakly modulated (Reppas, Niyogi, Dale, Sereno, & Tootell, 1997). All of these results suggest that the critical spatially limiting motion processing of non-overlapping, motion-defined surfaces takes place within lower-order areas such as V1 or V2.

How, then, does the visual cortex encode transparent motion? A common view is that motion transparency, as well as other structure-from-motion phenomena, is encoded at the level of MT (see Andersen, 1997). One experimental result taken as evidence for this hypothesis is the change of activity in some MT neurons, when presented with transparent stimuli. Snowden, Treue, Erickson, and Andersen (1991) first demonstrated that adding either non-overlapping or overlapping motion in the direction opposite the preferred direction largely decreases the responses of MT neurons to motion in their preferred direction. Because pairing both decreases MT activity in monkeys and blocks the perception of motion transparency in humans, yet produced little or no response change in V1 (Qian & Andersen, 1994), Qian and colleagues suggested that motion transparency is encoded at the level of MT. The discrepancy between the small V1-sized pairing distance that abolishes transparency and the lack of a pairing effect on V1 responses led Qian and Andersen (1994) to postulate that pairing might affect MT sub-units receiving inputs from motion-opponent V1 neurons (see Braddick & Qian, 2001 for a review).

However, several physiological and psychophysical results, including those in the present paper, are rather difficult to reconcile with this view. First, if transparency were encoded at the level of MT, one would expect the perceptual transition from corrugation to transparency to occur a much larger bar width. Although one could imagine that a population code might allow MT neurons, with their large receptive fields that increase rapidly with eccentricity, to none the less detect high-spatial frequency corrugation, it is difficult to explain how such a mechanism could produce the weak eccentricity dependence that we observed. Second, it is not clear that V1 neurons are actually unaffected by manipulations that affect the perception of transparency. Qian and Andersen (1995) followed up their earlier study by recording the response of V1 neurons to high-density (22 and 44 dots/deg^2) transparent random-dot patterns with opponent motion and to coun-

ter-phase gratings. Most V1 responses were significantly lower with opponent random-dot patterns than with uniform motion. These modulations were, however, not significantly different from the changes observed between the responses to a single moving grating and to a counter-phase grating. Since one display (opponent random dots) but not the other (counter-phase grating) is seen as transparent, Qian and Andersen (1995) concluded that V1 neurons cannot distinguish between perceptually transparent and non-transparent motion, but this evidence is less than overwhelming. Third, much like these V1 findings, Snowden et al. (1991) found that both overlapping (i.e. corrugated) and non-overlapping (i.e. transparent) motion displays lead to similar dramatic suppressive interactions at the level of MT neurons, so such effects do not provide strong evidence either for or against a link with the perception of transparency. Fourth, in humans, Reppas et al. (1997) found little fMRI activity elicited in area MT by transparent displays. Therefore, a critical reading of the current literature on the neural mechanisms for motion segmentation suggests that MT/V5 is not a good candidate and that V1 plays a central role. The present results, together with those of an earlier study (Masson et al., 1999), provide quantitative support for the hypothesis that motion segmentation is constrained by a segregation process that operates at a small spatial scale, over a restricted range of speeds, consistent with a limiting mechanism at the level of area V1. Such a hypothesis opens the door to future experimental work aiming to understand the interplay between areas V1 and MT in segmenting visual scenes (see Hupé et al., 1998, for example).

5. Conclusion

The pairing and corrugation effects observed in this study demonstrate that visual motion segregation based on speed cues alone is possible down to a spatial scale comparable to that of the receptive field size of V1 neurons. We also found that this critical spatial scale for accurate segmentation has the same dependence on eccentricity as V1 receptive fields. Lastly, the effect of dot density is also consistent with a segregation mechanism with a V1-like receptive-field size. It should be noted, however, that performance in many human spatial-vision tasks exhibits a similar V1-like dependence on eccentricity (see, for example, Virsu & Rovamo, 1979). Obviously, early spatial processing in the primary visual cortex constrains further processing along many visual dimensions (see Lennie, 1998 for a review). We have merely shown that speed segmentation follows this general pattern as well. The main point is that the fine spatial scale of human speed-segmentation is not limited by a mechanism with an MT-like receptive-field

size and therefore is not likely limited by processing within area MT. Local motion pooling within the segmentation mechanism may also explain the poorer segmentation performance observed with transparent, as opposed to corrugated, moving random-dot displays.

Appendix A. Stochastic model

To provide an explanation of the qualitative trends in our data, we propose the following simple model that estimates the speed-segmentation threshold variations as a function of bar width (B_w) within our square ($S \times S$) corrugated displays, given the angular size of the receptive field of the local pooling units (assumed for simplicity to be a $U \times U$ square), the total number of dots in the display (N), and the eccentricity (Ecc) of the center of the stimulus. We use the fact that, for visual area V1, U can be described by the following function (Dow et al., 1981):

$$U = 0.22 + 0.044 \cdot Ecc \tag{1}$$

We then simply assume that threshold elevation (THE) is the simple linear difference of the probability of 'interference' (P_{int}) and of 'cooperation' (P_{coop}) within the stimulus:

$$THE = P_{int} - P_{coop} \tag{2}$$

P_{int} is defined as the expected probability of having, within the same local pooling area, at least one dot moving at a speed of v_1 and at least one dot moving at the other speed v_2. This clearly happens near 'motion borders' when pooling units straddle a border. P_{coop} is defined as the expected probability of having, within the same local pooling area, more than one dot moving at the same speed. We make the further assumption that cooperation can only occur in stimulus regions where interference does not (i.e. interference trumps cooperation). Although Eq. (2) is arbitrary, it reflects the simple assumption that interference will raise thresholds and that cooperation will decrease them. We now distinguish between three possible cases:

A.1. Unit size is smaller or equal to the bar width ($U \leq B_w$) for paired or unpaired dots

To evaluate these probabilities, we define the local probability densities of interference (p_{int}) and of cooperation (p_{coop}) for a given possible position of a pooling unit. To compute P_{int} and P_{coop}, we integrated from $x = 0$ to B_w and then normalized over the bar width:

$$P_{int} = \int_0^{B_w} p_{int}\, dx \Big/ \int_0^{B_w} dx$$
$$P_{coop} = \int_0^{B_w} p_{coop}\, dx \Big/ \int_0^{B_w} dx \qquad (3)$$

with x defined as the position of the bottom edge of the unit in a coordinate system whose origin is the border with dots moving at v_2 above that border and at v_1 below it (Fig. 7a). The probability densities are first calculated as shown next.

In our displays, the total number of dots was evenly distributed among the bars. The number of dots within a bar is therefore:

$$N_b = \frac{N \times B_w}{S}. \qquad (4)$$

The probability of one of these uniformly distributed dots being within a particular subregion of the bar is the ratio of that region's area to the total bar area ($S.B_w$). The probability of at least one dot (necessarily moving at v_1) being in the portion of the unit below the border is 1 minus the probability of all N_b of the dots not being in a region of area $[\min(x,U)U]$:

$$p_{v1} = 1 - \left(1 - \frac{\min(x,U)\, U}{S \times B_w}\right)^{N_b}. \qquad (5)$$

Similarly, the probability of at least one dot (necessarily moving at v_2) being in the portion of the unit above the border is:

$$p_{v2} = 1 - \left(1 - \frac{\max(U - x, 0)\, U}{S \times B_w}\right)^{N_b}. \qquad (6)$$

Because these are independent events, the interference probability density is then just:

$$p_{int} = p_{v1} \times p_{v2}. \qquad (7)$$

Note that for $x > U$, $p_{V2} = 0$ and therefore $p_{int} = 0$ as we are outside of the 'interference' zone near the border.

The probability density of cooperation is the probability of having more than one dot within the local pooling unit's receptive field as long as it does not straddle a border. This is equivalent to one minus the probability of having exactly one or exactly no dots:

$$p_{coop} = \begin{cases} 1 - N_b \dfrac{U^2}{S \times B_w}\left(1 - \dfrac{U^2}{S \times B_w}\right)^{N_b - 1} - \left(1 - \dfrac{U^2}{S \times B_w}\right)^{N_b} & \text{if } x \geq U \\ 0 \ (\text{by assumption}) & \text{if } x < U \end{cases} \qquad (8)$$

A.2. Unit size is larger than the bar width ($U > B_w$) for unpaired dots

When the bar width is smaller than the unit size, we assume that there is no cooperation and that only interference is possible. The exact probability equations are however more complicated than for the case shown above. To simplify the calculations, we therefore took advantage of the fact that for, $B_w = U/n$ with n being an even number, exactly half of the unit's receptive field will be over even bars and half over odd bars. This situation is then equivalent to having each half of the local pooling area over a virtual bar of width $U/2$.

The number of dots within each virtual bar of width $U/2$ is:

$$N_{vb} = \frac{N \dfrac{U}{2}}{S}. \qquad (9)$$

Using the same logic as for Eqs. (5)–(7) above, the probability of interference is:

$$P_{int} = \left[1 - \left[1 - \frac{U \dfrac{U}{2}}{S \dfrac{U}{2}}\right]^{N_{vb}}\right]^2 = \left(1 - \left(1 - \frac{U}{S}\right)^{N_{vb}}\right)^2. \qquad (10)$$

We then evaluated Eq. (10) for $B_w = U/n$, with n being an even number, and interpolated to obtain the smooth curves in Fig. 7. These values represent a lower bound on threshold. The exact probabilities only meaningfully deviate for Eq. (10) for values of B_w less than but close to U, but this omitted detailed structure is unimportant given that our goal is merely to reproduce the overall trends.

A.3. Unit size is larger than the bar width ($U > B_w$) for paired dots

With bar width larger than the unit size, dot pairing has no effect, and the computations are identical for both paired and unpaired dots. With bar width smaller than U, the computation of P_{int} for paired dots is the same as that in Section 2 above, with one important difference. For unpaired displays, P_{v1} and P_{v2} are independent. With paired dots, $P_{v2|v1}$ is, by definition, equal to 1 (if there is a motion vector on one side of the border, there will be a paired one on the other side), and therefore:

$$P_{int} = 1 - \left(1 - \frac{U}{S}\right)^{N_{vb}}. \qquad (11)$$

References

Andersen, R. A. (1997). Neural mechanisms of visual motion perception in primates. *Neuron*, *18*, 865–872.

Albright, T. D., & Desimone, R. (1987). Local precision of visuotopic organization in the middle temporal area of the macaque. *Experimental Brain Research*, *65*, 582–592.

Albright, T. D., & Stoner, G. R. (1995). Visual motion perception. *Proceedings of the National Academy of Sciences, USA*, *92*, 2433–2440.

Braddick, O. J. (1993). Segmentation versus integration in visual motion processing. *Trends in Neurosciences*, *16*, 262–268.

Braddick, O. J. (1997). Local and global representations of velocity: transparency, opponency, and global direction perception. *Perception*, *26*, 995–1010.

Braddick, O. J., & Qian, N. (2001). The organization of global motion and transparency. In J. M. Zanker, & J. Zeil, *Motion vision. Computational, neural and ecological constraints* (pp. 85–112). Berlin: Springer.

Curran, W., & Braddick, O. J. (2000). Speed and direction of locally paired dot patterns. *Vision Research*, *40*, 2115–2124.

Donadio, G., Mestre, D. R., & Masson, G. S. (1998). Motion transparency perception in central and peripheral vision. *Perception*, *27*(S1), 187b.

Dow, B. M., Snyder, A. Z., Vautin, R. G., & Bauer, R. (1981). Magnification factor and receptive field size in foveal striate cortex of the monkey. *Experimental Brain Research*, *44*, 213–228.

Georgeson, M. A., Freeman, T. C. A., & Scott-Samuel, N. E. (1996). Sub-pixel accuracy: psychophysical validation of an algorithm for fine positioning and movements of dots on visual displays. *Vision Research*, *36*, 605–612.

Golomb, B., Andersen, R. A., Nakayama, K., MacLeod, D. I. A., & Wong, A. (1985). Visual thresholds for shearing motion in monkey and man. *Vision Research*, *25*, 813–820.

Hupé, J.-M., James, A. C., Payne, B. R., Lomber, S. G., Girard, P., & Bullier, J. (1998). Cortical feedback improves discrimination between figure and ground by V1, V2 and V3 neurons. *Nature*, *394*, 784–787.

Lamme, V. A., van Dijk, B. W., & Spekreijse, H. (1993). Contour from motion processing occurs in primary visual cortex. *Nature*, *363*, 541–543.

Lauwers, K., Saunders, R. C., Vogels, R., Vandenbussche, E., & Orban, G. (2000). Impairment in motion discrimination tasks is unrelated to amount of damage to superior temporal sulcus motion areas. *Journal of Comparative Neurology*, *420*, 539–557.

Leventhal, A. G., Wang, Y., Schmolesky, M. T., & Zhou, Y. (1998). Neural correlates of boundary perception. *Visual Neuroscience*, *15*, 1107–1118.

Lennie, P. (1998). Single units and visual cortical organization. *Perception*, *27*, 889–935.

McKee, S., & Nakayama, K. (1984). The detection of motion in the peripheral visual field. *Vision Research*, *24*, 25–32.

Marcar, V. L., & Cowey, A. (1992). The effects of removing superior cortical motion area in macaque monkey. II. Motion discrimination using random dot displays. *European Journal of Neuroscience*, *4*, 1228–1237.

Marcar, V. L., Raiguel, S. E., Xiao, D.-K., Maes, H., & Orban, G. A. (1995). Processing of kinetically defined boundaries in the cortical motion areas MT of macaque monkey. *Journal of Neurophysiology*, *74*, 1258–1270.

Marcar, V. L., Raiguel, S. E., Xiao, D., & Orban, G. A. (2000). Processing of kinetically defined boundaries in areas V1 and V2 of the macaque monkey. *Journal of Neurophysiology*, *84*, 2786–2798.

Masson, G. S., & Mestre, D. R. (1998). Motion segmentation from speed cues: effects of speed distribution, dot density and retinal eccentricity. *Perception*, *27*, 169b.

Masson, G. S., Mestre, D. R., & Stone, L. S. (1999). Speed tuning of motion segmentation and discrimination. *Vision Research*, *39*, 4299–4308.

Mather, G., & Moulden, B. (1980). Thresholds for movement direction: two directions are less detectable than one. *Quarterly Journal of Experimental Psychology*, *35*, 513–518.

Mestre, D., & Masson, G. (1998). Mechanisms of motion segmentation in corrugated and transparent motion displays. ARVO Annual Meeting, Fort Lauderdale, Florida, 10–15 May 1998. *Investigative Ophthalmology and Visual Sciences*, *39*, 4993.

Movshon, J. A., Adelson, E. H., Gizzi, M. S., & Newsome, W. T. (1985). The analysis of moving patterns. In C. Chagas, R. Gattass, & C. Gross, *Pattern recognition mechanisms* (pp. 117–151). Vatican City: Vatican Press.

Naka, K. I., & Rushton, W. A. (1966). S-potentials from color units in the retina of fish. *Journal of Physiology (London)*, *185*, 584–589.

Nakayama, K. (1981). Differential motion hyperacuity under conditions of common image motion. *Vision Research*, *21*, 1475–1482.

Nakayama, K., & Tyler, C. W. (1981). Psychophysical isolation of movement sensitivity by removal of familiar position cues. *Vision Research*, *21*, 427–433.

Nakayama, K., Silverman, G. H., MacLeod, D. I. A., & Mulligan, J. (1985). Sensitivity to shearing and compressive motion in random dots. *Perception*, *14*, 225–238.

Nawrot, M., & Sekuler, R. (1990). Assimilation and contrast in motion perception: Exploration in cooperativity. Vision Research, 30, 1439–1451.

Qian, N., & Andersen, R. A. (1994). Transparent motion perception as detection of unbalanced motion signals. II. Physiology. *Journal of Neuroscience*, *14*, 7367–7380.

Qian, N., Andersen, R. A., & Adelson, E. H. (1994a). Transparent motion perception as detection of unbalanced motion signals. I. Psychophysics. *Journal of Neuroscience*, *14*, 7357–7366.

Qian, N., Andersen, R. A., & Adelson, E. H. (1994b). Transparent motion perception as detection of unbalanced motion signals. III. Modeling. *Journal of Neuroscience*, *14*, 7381–7392.

Qian, N., & Andersen, R. A. (1995). V1 responses to transparent and nontransparent motions. *Experimental Brain Research*, *103*, 41–50.

Reppas, J. B., Niyogi, S., Dale, A. M., Sereno, M. I., & Tootell, R. B. (1997). Representation of motion boundaries in retinotopic human visual cortical areas. *Nature*, *368*, 175–179.

Sachtler, W. L., & Zaidi, Q. (1995). Visual processing of motion boundaries. *Vision Research*, *35*, 807–826.

Smith, A. T., Curran, W., & Braddick, O. J. (1999). What motion distributions yield global transparency and spatial segmentation? *Vision Research*, *39*, 1121–1132.

Snowden, R. J. (1992). Sensitivity to relative and absolute motion. *Perception*, *21*, 563–568.

Snowden, R. J. (1989). Motions in orthogonal direction are mutually suppressive. *Journal of the Optical Society of America A*, *7*, 1096–1101.

Snowden, R. J., Treue, S., Erickson, R. E., & Andersen, R. A. (1991). The response of area MT and V1 neurons to transparent motion. *Journal of Neuroscience*, *11*, 2768–2785.

Taylor, M. M., & Creelman, C. D. (1967). PEST: efficient estimation on probability functions. *Journal of the Acoustical Society of America*, *41*, 782–787.

van Doorn, A. J., & Koenderink, J. J. (1982a). Visibility of movement gradients. *Biological Cybernetics*, *44*, 167–175.

van Doorn, A. J., & Koenderink, J. J. (1982b). Spatial properties of the visual detectability of moving spatial white noise. *Experimental Brain Research*, *45*, 189–195.

van Doorn, A. J., & Koenderink, J. J. (1983). Detectability of velocity gradients in moving random-dot patterns. *Vision Research*, *23*, 799–804.

Virsu, V., & Rovamo, J. (1979). Visual resolution, contrast sensitivity, and the cortical magnification factor. *Experimental Brain Research*, *37*, 475–494.

Watson, A. B., & Eckert, M. P. (1994). Motion-contrast sensitivity: visibility of motion gradients of various spatial frequencies. *Journal of the Optical Society of America*, *11*, 496–505.

Wishart, K. A., & Braddick, O. J. (1997). Performance-based measures of transparency in locally-balanced motions. *Perception*, *26*(Suppl. 1), 88.